crystals

MDPI

Article

Formation of $LiNbO_3$ Nanocrystals Using the Solvothermal Method

Gabriella Dravecz [1,*], Tamás Kolonits [2,3] and László Péter [1]

[1] Wigner Reseach Centre for Physics, Konkoly-Thege Miklós út 29–33, H-1121 Budapest, Hungary
[2] Institute for Technical Physics and Materials Science, Centre for Energy Research, Eötvös Loránd Research Network, Konkoly-Thege Miklós út 29–33, H-1121 Budapest, Hungary
[3] Department of Materials Physics, ELTE Eötvös Loránd University, Pázmány Péter sétány 1/A, H-1117 Budapest, Hungary
* Correspondence: dravecz.gabriella@wigner.hu

Abstract: The optimization of the parameters of the solvothermal synthesis of lithium niobate ($LiNbO_3$, LN) nanocrystals from Nb_2O_5 and LiOH was performed. The effects of polyol media, reaction time and Li excess of the starting reagents were investigated. According to the X-ray diffraction phase analysis, Li_3NbO_4 and Nb_2O_5 were also detected besides the LN phase in many samples depending on the ratio of the starting components and the reaction time. The best yield and the most homogeneous LN phase was prepared by using diethylene glycol medium with a Li/Nb ratio of 1.5 and a 72 h reaction time. The size and the shape of the LN particles were characterized by scanning electron microscopy. The particle size distribution was narrow and under 100 nm for all cases.

Keywords: $LiNbO_3$; nanocrystal; solvothermal method; X-ray method; electron microscopy

check for updates

Citation: Dravecz, G.; Kolonits, T.; Péter, L. Formation of $LiNbO_3$ Nanocrystals Using the Solvothermal Method. *Crystals* **2023**, *13*, 77. https://doi.org/10.3390/cryst13010077

Academic Editor: Bo Chen

Received: 6 December 2022
Revised: 23 December 2022
Accepted: 29 December 2022
Published: 1 January 2023

1. Introduction

Single-crystal lithium niobate is an often-used, highly investigated optical material with excellent nonlinear, acousto-optical, electro-optical and photorefractive properties [1]. The research of pure and rare-earth-doped nano-sized $LiNbO_3$ has shown growing interest in the past few years. It can be used, for example, in deep tissue imaging, diagnostics, and optical calibration and nanophotonics [2,3]. In the nanoscale region, the rare-earth dopant can act as a single photon source [4].

High-energy bal lmilling of either bulk $LiNbO_3$ crystals [5] or Li_2O/Nb_2O_5 [6] mixtures is a top-down method for preparing $LiNbO_3$ nanoparticles. The chemical bottom-up synthesis of $LiNbO_3$ nanoparticles has already been performed by the application of several methods [7] such as solid-state reactions [8] and solvothermal synthesis [9–15]. Kalinnikov et al. [16] prepared $LiNbO_3$ from peroxide solutions, but Li_3NbO_4 and $LiNb_3O_8$ phases also appeared in their product. A modified Pechini polymeric precursor method was elaborated [17] using Li_2CO_3 and ammonium niobate oxalate hydrate ($C_4H_4NNbO_9 \cdot xH_2O$) as the starting materials, requiring a 500 °C calcination temperature.

The preparation of thin LN films and powders by the sol-gel process has also been reported [18–21]. These synthesis routes often work at high temperatures, with the usual problem of the agglomeration of the particles and the high cost of the reactant(s). For solvothermal synthesis, the advantage of the water solubility of Li compounds was utilized and, generally, the hydrothermal method was chosen. In these methods, the reaction takes place in water, which limits the variability of the reaction parameters. A great variety of the $MeTrO_3$ compounds such as alkali (Na, K) niobates and tantalates have been prepared by the hydrothermal method to study their photocatalytic activity [22]. A microwave-assisted hydrothermal method was also optimized for preparing $K_{0.5}Na_{0.5}NbO_3$ [23,24].

The solvothermal synthesis using different organic media is an easy and effective way for producing nanoparticles at a relatively low temperature in a thermal autoclave

where the organic medium (ethylene glycol, diethylene glycol, glycerol, etc.) acting as stabilizer can control the growth of the particles and prevent their agglomeration [25]. Besides the shape and size regulation of the particles being formed, the above-mentioned media make it possible to reduce the pressure of the synthesis due to their relatively low vapor pressure compared to water. Several types of nanotubes (such as $NaNbO_3$ [26]), bismuth nanowires [27] and other nanostructured materials (hydrozincite ($Zn_5(CO_3)_2(OH)_6$) microspheres [28], metal oxides [29], $KNbO_3$ fine powders [30]) were produced successfully by the solvothermal method. Nakashima et. al. [31] tried lots of solvothermal media (alcohols) and synthetized $KNbO_3$ nanotubes. Gu et al. [32] prepared $NaNbO_3$ nanowires successfully using ethylene glycol as a polyol medium. $LiNbO_3$ has already been prepared by the solvothermal route [33] at a relatively high temperature (345 °C), although unreacted Nb_2O_5 residue was detected in the product.

In the present work, we apply several commonly used polyol media for optimizing solvothermal synthesis in order to find an easy, low-cost way at a relatively low temperature for preparing $LiNbO_3$ nanocrystals with a high yield and sufficient purity. It was our goal to replace solvents with high vapor tension (such as water and primary alcohols) with less volatile solvents in order to reduce the pressure during the synthesis. The samples were investigated by scanning electron microscopy (SEM), energy dispersive X-ray spectroscopy (EDS), dynamic light scattering (DLS) and X-ray diffraction (XRD) phase analysis.

2. Materials and Methods

2.1. Materials

The reagents: Nb_2O_5 (Starck, LN grade, 99.99%), $LiOH{\cdot}H_2O$ (98%, Alfa Aesar), ethylene glycol, EG (G. R., Lach:ner), diethylene glycol, dEG (puriss, Austranal), triethylene glycol, tEG (purum) and glycerol (87%, Finomvegyszer Szövetkezet Budapest) were used without further purification. The high-purity deionized water was provided by the ELGA Purelab Option 7 device.

Nb_2O_5 was pre-treated by milling the raw material down to 300–500 nm in particle diameter using a Fritsch Pulverisette 7 Premium line planetary mill (zirconia vial, 70 g zirconia balls of 3 mm, 1100 rpm, 10 min, 5g Nb_2O_5, 10 mL distilled water). Without this treatment, the product retained the original columnar structure of Nb_2O_5 and the LN formation could only be completed on its surface.

2.2. Synthesis Route

The reaction was performed through the following process:

$$Nb_2O_5 + 2LiOH \rightarrow 2LiNbO_3 + H_2O \quad (1)$$

1.09 mmol Nb_2O_5 was dispersed with the solution of $LiOH{\cdot}H_2O$ in a Teflon-lined hydrothermal autoclave prepared with 20 mL solvent of either EG, dEG, tEG or Glycerol. The Li/Nb (r) atomic ratio was 1.0 (1.25 and 1.5 were also tried for ethylene- and diethylene glycol). As it is shown later, the latter solvents exhibited the smallest ratio of unwanted product; therefore, they were selected to change the component ratio to 1.0, 1.25 and 1.5. The mixtures were annealed at 220 °C for 24, 48 or 72 h. After they cooled down to room temperature, the solid reaction product was separated from the liquid medium by centrifugation. The residues of the polyol solvent, together with the excess dissolved Li salt, was removed by washing the samples with deionized water (decantation). The morphology of the dried powder was investigated by SEM and the formed phases were identified by XRD measurements. The yield of the reaction (η) was calculated using Equation (2)

$$\eta = \frac{m_1}{m_2} \times 100 \quad (2)$$

where m_1 is the mass of $LiNbO_3$ after the solvothermal reaction from three parallel mass measurements for the optimized case (the Nb_2O_5 residue in the product was neglected), and m_2 is the calculated mass of $LiNbO_3$ assuming a complete reaction.

2.3. Characterization of the Materials Synthesized

Dynamic light scattering measurements were performed using Malvern Zetasizer Nano S, Worcestershire, UK in the 0.1–10000 nm range for determining the size distribution of the products.

X-ray diffractometry (XRD) measurements were performed by a Rigaku (Tokyo, Japan) Smartlab X-ray diffractometer with CuKα radiation (wavelength: λ = 0.15418 nm). The measurements were taken in Bragg–Brentano geometry.

Scanning electron microscopy—A TESCAN MIRA3 scanning electron microscope was used for imaging the particles produced by the ball-milling procedure. The optimum of the acceleration voltage for the imaging of LN particles with secondary electrons was found to be 12 kV. Possible contamination of Zr from the vial was checked by the same electron microscope with an EDAX Element energy dispersive X-ray spectrometer (EDS). The elemental analysis was carried out at 30 kV acceleration voltage, making it also possible to detect the K-lines of both Nb and Zr around 18 keV.

3. Results and Discussion

3.1. Morphology and Size Distribution of $LiNbO_3$ Nanocrystals

The SEM investigations were performed to characterize the morphology and size distribution of the samples. The raw material of Nb_2O_5 has a column structure (Figure 1a). Using it for the solvothermal reaction without any pre-treatment resulted in column-structured products (Figure 1b). As the SEM micrographs in Figure 1 show, the majority of the starting niobium(V) oxide grains larger than about half of a micrometer retained their shape; hence, the reaction did not take place via the dissolution of Nb_2O_5.

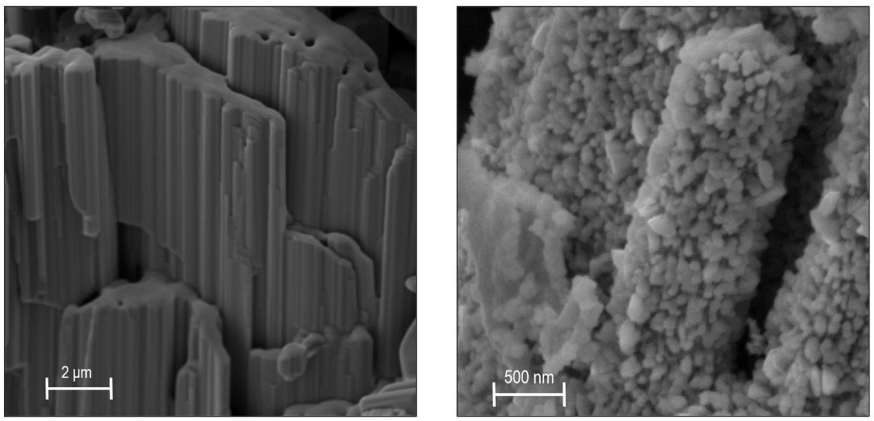

Figure 1. SEM images showing the columnar structure of the Nb_2O_5 raw material (**a**) and the product after the solvothermal reaction using the Nb_2O_5 without pre-milling (**b**).

For the above reasons, the Nb_2O_5 starting material was ball-milled before using it for the solvothermal reaction until its column structure disappeared. In all cases, using milled Nb_2O_5, regardless of the quality and quantity of the formed phases, the product of the solvothermal reaction showed a homogeneous morphology with a particle size under 100 nm (Figure 2).

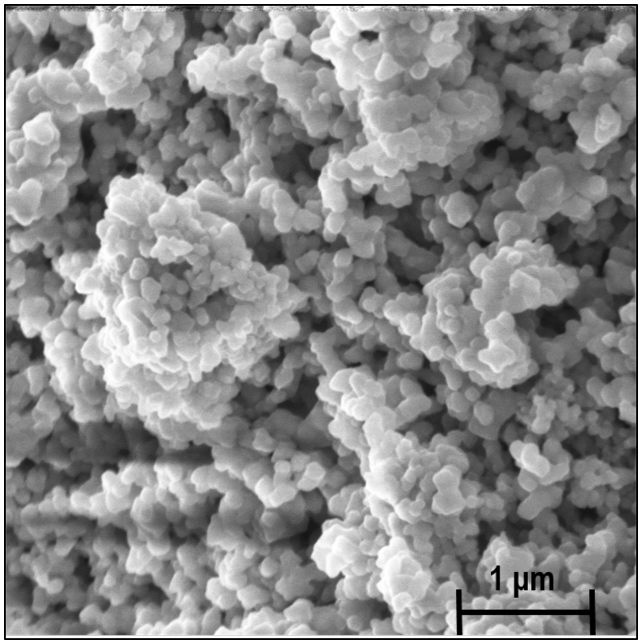

Figure 2. Typical SEM image of the LN samples prepared by the solvothermal synthesis by using pre-milled Nb_2O_5 as solid reactant.

The size distribution of the particles was followed by DLS measurements (Figure 3). The shape and the position of the curves were found to be quite similar, so only the samples treated for 72 h and with the highest starting *r* are shown.

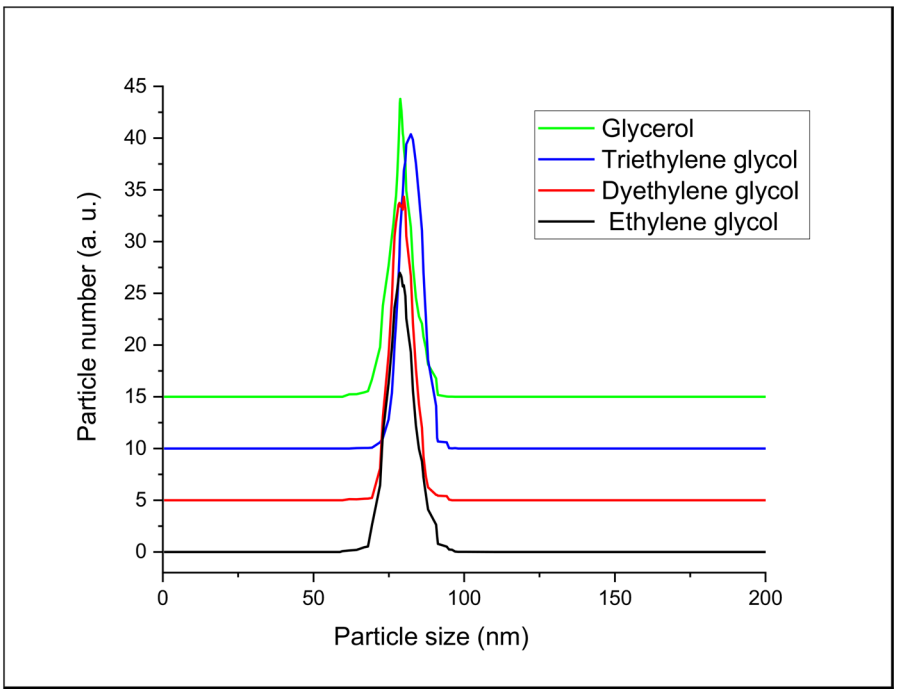

Figure 3. Size distribution of the nanoparticles after the synthesis. Curves are displaced by a multiple of five units each along the ordinate for the sake of clarity.

According to the DLS measurements, the diameter of the particles produced by the solvothermal methods are in the range of 60–100 nm, which shows a good agreement with the SEM analysis.

3.2. Phase Identification of $LiNbO_3$ Nanocrystals

XRD phase analysis revealed three different phases in the samples: the desired $LiNbO_3$, the residue of the starting Nb_2O_5 and a Li-rich phase identified as Li_3NbO_4. With the correct choice of the synthesis parameters, the amount of the latter two phases could be dramatically decreased, as shown in Table 1.

Table 1. The parameters of synthesis (polyol used, reaction time and *r*) and the intensity ratio of selected diffraction peaks of Li_3NbO_4 and $LiNbO_3$ phases. The presence/absence of observable amount of remnant Nb_2O_5 is noted by +/− sign. With the optimized reaction parameters (marked by bold and underlined), the $LiNbO_3$ phase could only be detected.

Polyol	Reaction Time (h)	r	$I(Li_3NbO_4)/I(LiNbO_3)$	Nb_2O_5
Ethylene glycol	24	1	4.81	+
	48	1	2.29	+
	72	1	2.69	+
		1.25	2.33	+
		1.5	1.52	+
Diethylene glycol	24	1	0.81	+
	48	1	0.72	+
	72	1	0.1	+
		1.25	0.00	+
		1.5	0.00	-
Triethylene glycol	24	1	26.85	+
	48	1	11.00	+
	72	1	3.30	+
Glycerol	24	1	7.83	+
	48	1	3.69	+
	72	1	2.09	+

It has to be noted that the Li-rich phase is not exactly stoichiometric Li_3NbO_4, and the exact composition of this phase may vary between the different samples. Therefore, a quantitative analysis of the amount of the phases is not possible (i.e., the intensity of the diffraction peaks associated with this phase does not solely depend on the amount of this phase but on the exact composition, too). The proportion of Li_3NbO_4 and $LiNbO_3$ in the product was characterized by the intensity ratio of the corresponding diffraction peaks of each phase (13.4° and 14.2° for Li_3NbO_4, while 56.1° and 56.7° for $LiNbO_3$).

3.2.1. Effect of the Reaction Time

As shown in Table 1, the amount of the Li-rich Li_3NbO_4 phase compared to $LiNbO_3$ decreases with increasing reaction time. In addition, as demonstrated in Figure 4, the amount of residual Nb_2O_5 also decreases with the increasing reaction time. This result suggests that the reaction described by Equation (1) goes through two consecutive steps. First, LiOH reacts with Nb_2O_5 on the surface of the nanoparticles, forming the Li-rich Li_3NbO_4 phase:

$$Nb_2O_5 + 6LiOH \rightarrow 2Li_3NbO_4 + 3H_2O \quad (3)$$

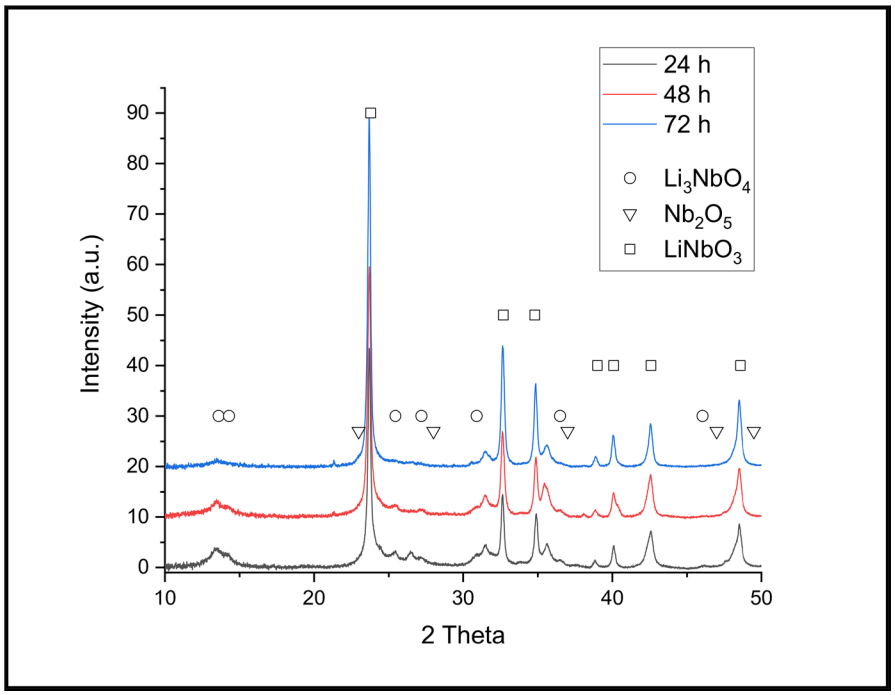

Figure 4. Effect of the reaction time on the chemical synthesis of LN as shown by the XRD diffractograms (the fixed synthesis parameters for the different samples were diethylene glycol as solvent and $r = 1$). The intensity of the diffraction peaks corresponding to the Li_3NbO_4 phase decreases with the increasing reaction time. A similar trend could be observed in the case of the other time triplets.

Then, the second step is that the Li_2O already incorporated to the peripheral Li_3NbO_4 phase penetrates further into the Nb_2O_5 particle and forms lithium niobate:

$$Li_3NbO_4 + Nb_2O_5 \rightarrow 3LiNbO_3 \quad (4)$$

Since the rate of reaction three is limited by solid-state diffusion, an observable amount of the metastable Li_3NbO_4 phase could remain in the sample if the time of the heat treatment is not long enough. Figure 3 shows that, with the increase in the reaction time, the amount of Li_3NbO_4 decreases. This trend is the same for all the time triplets of the samples (Table 1). Reaction times of 24 or 48 h were not sufficient for accomplishing the solid-state reaction; therefore, the raw material, Nb_2O_5, was found in these products. For EG and dEG, 72 h was found to be enough for completing the LN formation.

It appears that reaction two is an "uphill" process in the sense that the ingress of the lithium oxide into the Nb_2O_5 phase is much more intense than what is needed for the formation of any solid phase with relatively little lithium content (such as $LiNb_3O_8$ or $LiNbO_3$). The driving force of the "supersaturation" of the solid material with the lithium-rich Li_3NbO_4 phase could be that the lithium oxide uptake requires a significant redistribution of the Nb_2O_5 lattice. Once the original crystal lattice is expanded by some lithium oxide uptake, the further ingress of lithium oxide is relatively less hindered than the transformation of the neighboring Nb_2O_5 zone, with the crystal structure yet unchanged. After a sufficiently long time, the composition of the grains is levelled off. Although it is hard to find any explanation for why and how the solid-state processes can depend on the solvent quality, the component ratios, as shown in Table 1, unambiguously indicate that the solvent plays a crucial role in the formation rate of the final product.

The appearance of the Li_3NbO_4 phase and the absence of the $LiNb_3O_8$ phase indicate that the lithium oxide uptake during the solvothermal synthesis is fundamentally different than the lithium oxide release and uptake of $LiNbO_3$. With an appropriate heat treatment and lithium oxide vapor pressure, the lithium oxide content of LN can be finely tuned (like the congruent $\rightarrow$ stoichiometric transition with some 1.6 mol% Li_2O uptake). In this

process, the Li_3NbO_4 phase does not appear prior to the saturation of LN with Li_2O. The explanation of the difference lies in the role of the mechanochemical effect, which is high when the Nb_2O_5 phase is transformed to LN and insignificant when the niobate structure is already present.

3.2.2. Effect of the Polyol Medium

Using EG or dEG, the phases found under the identical reaction circumstances were the same with very similar peak intensities in the diffractograms. In these cases, we could find optimal parameters for LN forming. Using tEG or glycerol as reaction media, a significant amount of initial Nb_2O_5 phase was found in the product because the reaction could not be completed at this temperature (220 °C) during 72 h. Figure 5 shows the identified phases after the 72 h reaction time.

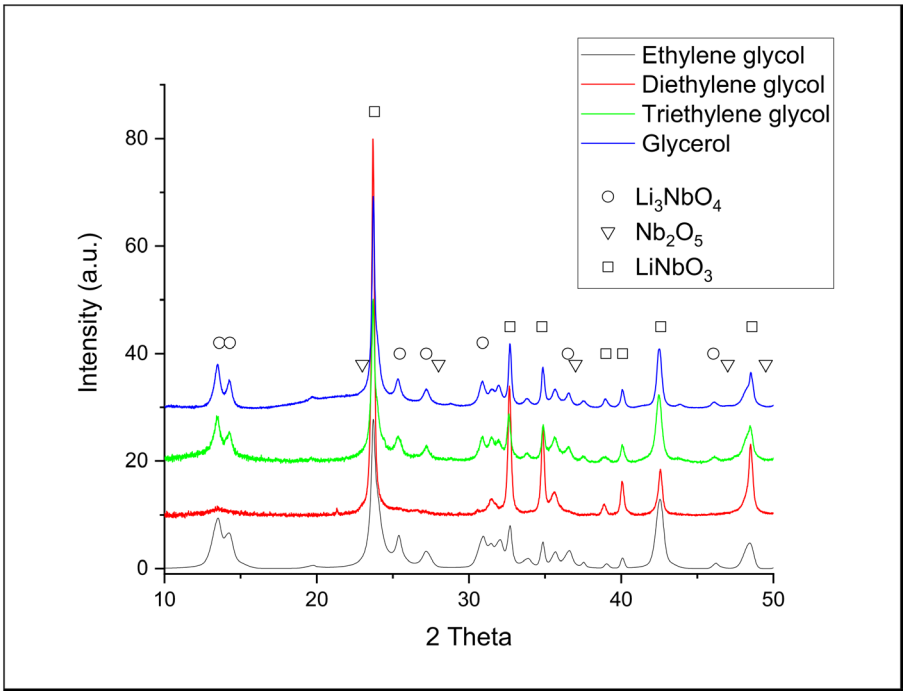

Figure 5. Effect of the polyol medium for the chemical synthesis of LN as shown by the XRD diffractograms (r = 1 and all samples were treated for 72 h).

3.2.3. Effect of the Li/Nb Atomic Ratio

During the experiments with the r = 1 in the starting mixture, the Nb_2O_5 phase could not completely disappear. The research hypothesis was that, with the consumption of the LiOH in the liquid medium, the driving force of the lithium oxide uptake of the solid phase decreased so much that the process essentially stopped. For this reason, for the dEG (i.e., for the solvent by using which the Li-rich phase was the least abundant already at the smallest reaction time), different r were tried. The optimal reactant ratio was found to be 1.5, where the Nb_2O_5 phase completely disappeared. Figure 6 shows this result through the X-ray diffractograms of the three samples.

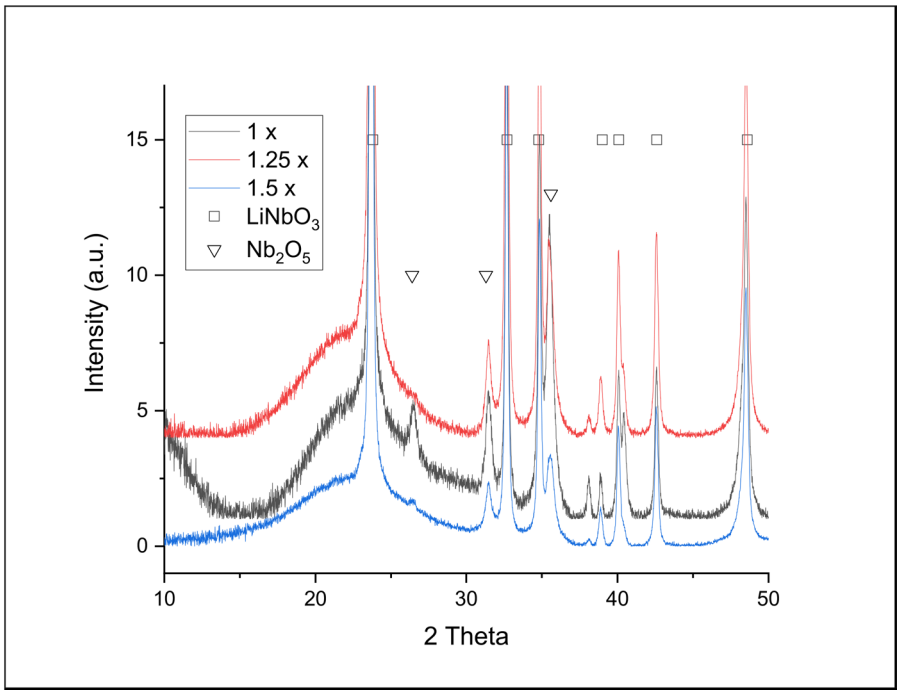

Figure 6. Effect of the Li excess on the chemical synthesis of LN showed through XRD diffractograms (the fixed parameters for the synthesis of different samples were as follows: diethylene glycol solvent, 72 h reaction time).

4. Conclusions

An easy, relatively low-temperature and moderate-pressure solvothermal method was optimized for preparing $LiNbO_3$ nanocrystals with a homogenous particle size distribution between 60–100 nm with a yield of 90%. At 220 °C, the optimal synthesis parameters for the reaction of Nb_2O_5 with LiOH to form $LiNbO_3$ were found to be diethylene glycol as the polyol medium, a 72 h reaction time and r = 1.5. Independently of the polyol medium used, the lithium oxide uptake of the niobium(V) oxide grains started with the formation of a lithium-rich phase, Li_3NbO_4, very likely at the Nb_2O_5/solvent boundary, which was followed by the equilibration of the concentrations within the grains. For the accomplishment of the $LiNbO_3$ formation, a lithium oxide excess was necessary.

Author Contributions: Conceptualization, G.D. and L.P.; methodology, L.P.; software, G.D. and T.K.; validation, G.D., T.K. and L.P.; formal analysis, L.P.; investigation, G.D., T.K. and L.P.; resources, G.D., T.K. and L.P.; data curation, G.D. and T.K.; writing—original draft preparation, G.D.; writing—review and editing, T.K. and L.P.; visualization, G.D.; supervision, L.P.; project administration, G.D.; funding acquisition, G.D., T.K. and L.P. All authors have read and agreed to the published version of the manuscript.

Funding: This research was funded by the National Research, Development and Innovation Fund of Hungary (OTKA 134921) and by the Ministry of Innovation and Technology and the National Research, Development and Innovation Office within the Quantum Information National Laboratory of Hungary.

Acknowledgments: László Kovács (Wigner Research Centre for Physics, Hungary) is acknowledged for the professional consultation and proofreading the manuscript.

Conflicts of Interest: The authors declare no conflict of interest.

References

1. Kovács, L.; Corradi, G. New Trends in Lithium Niobate: From Bulk to Nanocrystals. *Crystals* **2021**, *11*, 1356. [CrossRef]
2. Vittadello, L.; Klenen, J.; Koempe, K.; Kocsor, L.; Szaller, Z.; Imlau, M. NIR-to-NIR Imaging: Extended Excitation Up to 2.2 µm Using Harmonic Nanoparticles with a Tunable high Energy (TIGER) Widefield Microscope. *Nanomaterials* **2021**, *11*, 3193. [CrossRef]

3. Kijatkin, C.; Bourdon, B.; Klenen, J.; Kocsor, L.; Szaller, Z.; Imlau, M. Time-Resolved Nonlinear Diffuse Femtosecond-Pulse Reflectometry Using Lithium Niobate Nanoparticles with Two Pulses of Different Colors. *Adv. Photonics Res.* **2021**, *2*, 2000019–2000026. [CrossRef]
4. Dibos, A.M.; Raha, M.; Phenicie, C.M.; Thompson, J.D. Atomic Source of Single Photons in the Telecom Band. *Phys. Rev. Lett.* **2018**, *120*, 243601–243607. [CrossRef]
5. Kocsor, L.; Péter, L.; Corradi, G.; Kis, Z.; Gubicza, J.; Kovács, L. Mechanochemical reactions of lithium niobate induced by high-energy ball-milling. *Crystals* **2019**, *9*, 334. [CrossRef]
6. Luo, J.H. Preparation of Lithium Niobate Powders by Mechanochemical Process. *Appl. Mech. Mater.* **2011**, *121–126*, 3401–3405. [CrossRef]
7. Debnath, C.; Kar, S.; Verma, S.; Bartwal, K.S. Synthesis of Lithium Niobate Nanoparticles. *Encycl. Nanosci. Nanotechnol.* **2018**, *30*, 295–326.
8. Barik, R.; Satpathy, S.K.; Behera, B.; Biswal, S.K.; Mohapatra, R.K. Synthesis and spectral Characterizations of nano sized Lithium Niobate ($LiNbO_3$) Ceramic. *Micro Nanosyst.* **2020**, *12*, 81–87. [CrossRef]
9. An, C.; Tang, K.; Wang, C.; Shen, G.; Jin, Y.; Qian, Y. Characterization of $LiNbO_3$ nanocrystals prepared via a convenient hydrothermal route. *Mater. Res. Bull.* **2002**, *37*, 1791–1796. [CrossRef]
10. Luo, C.; Xue, D. Mild, Quasireverse Emulsion Route to Submicrometer Lithium Niobate Hollow Spheres. *Langmuir* **2006**, *22*, 9914–9918. [CrossRef]
11. Yu, J.; Liu, X. Hydrothermal synthesis and characterization of $LiNbO_3$ crystal. *Mater. Lett.* **2007**, *61*, 355–358. [CrossRef]
12. Liu, M.; Xue, D. Amine-Assisted Route To Fabricate $LiNbO_3$ Particles with a Tunable Shape. *J. Phys. Chem. C* **2008**, *112*, 6346–6351. [CrossRef]
13. Grange, R.; Choi, J.-W.; Hsieh, C.-L.; Pu, Y.; Magrez, A.; Smajda, R.; Forró, L.; Psaltis, D. Lithium niobate nanowires synthesis, optical properties, and manipulation. *Appl. Phys. Lett.* **2009**, *95*, 143105–143109. [CrossRef]
14. Huang, J.; Chen, Z.; Zhang, Z.; Zhu, C.; He, H.; Ye, Z.; Qu, G.; Tong, L. Synthesis and waveguiding of singlecrystalline $LiNbO_3$ nanorods. *Appl. Phys. Lett.* **2011**, *98*, 093102–093106. [CrossRef]
15. Zhan, J.; Liu, D.; Du, W.; Wang, Z.; Wang, P.; Cheng, H.; Huang, B.; Jiang, M. Synthesis and characterization of high crystallinity, well-defined morphology stoichiometric lithium niobate nanocrystalline. *J. Cryst. Growth* **2011**, *318*, 1121–1124. [CrossRef]
16. Kalinnikov, V.T.; Gromov, O.G.; Kunshina, G.B.; Kuzmin, A.P.; Lokshin, E.P.; Ivanenko, V.I. Preparation of $LiTaO_3$, $LiNbO_3$, and $NaNbO_3$ from Peroxide Solutions. *Inorg. Mater.* **2004**, *40*, 411–414. [CrossRef]
17. Yerlikaya, C.; Ullah, N.; Kamali, A.R.; Kumar, R.V. Size-controllable synthesis of lithium niobate nanocrystals using modified Pechini polymeric precursor method. *J. Therm. Anal. Calorim.* **2016**, *125*, 17–22. [CrossRef]
18. Gaeeni, M.R.; Bakouei, A.; Ghamsari, M.S. Highly Stable Colloidal Lithium Niobate Nanocrystals with Strong Violet and Blue Emission. *Inorg. Chem.* **2022**, *61*, 12886–12895. [CrossRef]
19. Zeng, H.C.; Tung, S.K. Synthesis of Lithium Niobate Gels Using a Metal Alkoxide—Metal Nitrate Precursor. *Chem. Mater.* **1996**, *8*, 2667–2672. [CrossRef]
20. Wang, L.H.; Yuan, D.R.; Duan, X.L.; Wang, X.Q.; Yu, F.P. Synthesis and Characterization of Fine Lithium Niobate Powders by Sol-Gel Method. *Cryst. Res. Technol.* **2007**, *42*, 321–324. [CrossRef]
21. Fakhri, M.A.; Salim, E.T.; Wahid, M.; Salim, Z.T.; Hashim, U. A novel parameter effects on optical properties of the $LiNbO_3$ films using sol-gel method. *AIP Conf. Proc.* **2020**, *2213*, 020242–020248.
22. Liu, J.W.; Chena, G.; Lia, Z.H.; Zhang, Z.G. Hydrothermal synthesis and photocatalytic properties of $ATaO_3$ and $ANbO_3$ (A = Na and K). *Int. J. Hydrogen Energy* **2007**, *32*, 2269–2272. [CrossRef]
23. Dumitrescu, C.-R.; Surdu, V.-A.; Stroescu, H.; Nicoara, A.-I.; Neacsu, I.A.; Trusca, R.; Andronescu, E.; Ciocan, L.T. Alkali Niobate Powder Synthesis Using an Emerging Microwave-Assisted Hydrothermal Method. *Materials* **2022**, *15*, 5410. [CrossRef] [PubMed]
24. Li, H.; Yan, Y.; Wang, G.; Li, Q.; Gu, Y.; Huang, J. Hydrothermal solvothermal synthesis potassium sodium niobate lead-free piezoelectric ceramics assisted with microwave. *J. Mater. Sci. Mater. Electron.* **2018**, *29*, 746–752. [CrossRef]
25. Cushing, B.L.; Kolesnichenko, V.L.; O'Connor, C.J. Recent Advances in the Liquid-Phase Syntheses of Inorganic Nanoparticles. *Chem. Rev.* **2004**, *104*, 3893–3946. [CrossRef] [PubMed]
26. Nakashima, K.; Toshima, Y.; Kobayashi, Y.; Ishikawa, Y.; Kakihana, M. Solvothermal synthesis and morphology control of $NaNbO_3$ nanotubes using a reaction medium of water and/or methanol. *J. Asian Ceram. Soc.* **2019**, *7*, 544–552. [CrossRef]
27. Wang, J.; Wang, X.; Peng, Q.; Li, Y. Synthesis and Characterization of Bismuth Single-Crystalline Nanowires and Nanospheres. *Inorg. Chem.* **2004**, *43*, 7552–7556. [CrossRef]
28. Yan, C.; Xue, D. Morphosynthesis of Hierarchical Hydrozincite with Tunable Surface Architectures and Hollow Zinc Oxide. *J. Phys. Chem. B* **2006**, *110*, 11076–11080. [CrossRef]
29. Yan, C.; Xue, D. General, Spontaneous Ion Replacement Reaction for the Synthesis of Micro- and Nanostructured Metal Oxides. *J. Phys. Chem. B* **2006**, *110*, 1581–1586. [CrossRef]
30. Jinachai, K.; Ngamjarurojana, A.; Rujiwatra, A. Solvothermal Synthesis, Sintering Behavior and Dielectric Properties of Potassium Niobate Fine Powders. *Chiang Mai J. Sci.* **2011**, *38*, 252–262.
31. Nakashima, K.; Ueno, S.; Wada, S. Solvothermal synthesis of $KNbO_3$ nanocubes using various organic solvents. *J. Ceram. Soc. Jpn.* **2014**, *122*, 547–551. [CrossRef]

32. Gu, Q.; Zhu, K.; Zhang, N.; Sun, Q.; Liu, P.; Liu, J.; Wang, J.; Li, Z. Modified Solvothermal Strategy for Straightforward Synthesis of Cubic $NaNbO_3$ Nanowires with Enhanced Photocatalytic H_2 Evolution. *J. Phys. Chem. C* **2015**, *119*, 25956–25964. [CrossRef]
33. Liu, M.; Xue, D. A solvothermal route to crystalline lithium niobate. *Mater. Lett.* **2005**, *59*, 2908–2910. [CrossRef]